SUPPORTING INFORMATION

Iridium(III) complexes with enhanced film amorphism as guests for efficient orange solution-processed single-layer PhOLEDs with low efficiency roll-off

Jun Dai,[1a] Kaifeng Zhou,[2a] Ming Li,[1] Huiqin Sun,[4] Yunqing Chen,[1] Shijian Su,*[2] Xuemei Pu,[1] Yan Huang*[1] and Zhiyun Lu*[1,3]

[1]College of Chemistry, Sichuan University, Chengdu, 610064, P. R. China

[2]State Key Laboratory of Luminescent Materials and Devices (South China University of Technology) and Institute of Polymer Optoelectronic Materials and Devices, South China University of Technology, Guangzhou 510640, P. R. China

[3]Key Laboratory of Green Chemistry and Technology, Minister of Education, Sichuan University, Chengdu, 610064, P. R. China

[4]Analytical and Testing Center, Sichuan University, Chengdu, 610064, P. R. China

[a] These authors contribute equally to this article

* To whom correspondence should be addressed. Fax: +86-28-85410059;

email: luzhiyun@scu.edu.cn (Z. Y. Lu); huangyan@scu.edu.cn (Y. Huang)

* To whom correspondence should be addressed. Fax: +86-20-87110606;

email: mssjsu@scut.edu.cn (S. J. Su)

Figure S1. XRD spectrum of the blank quartz substrate.

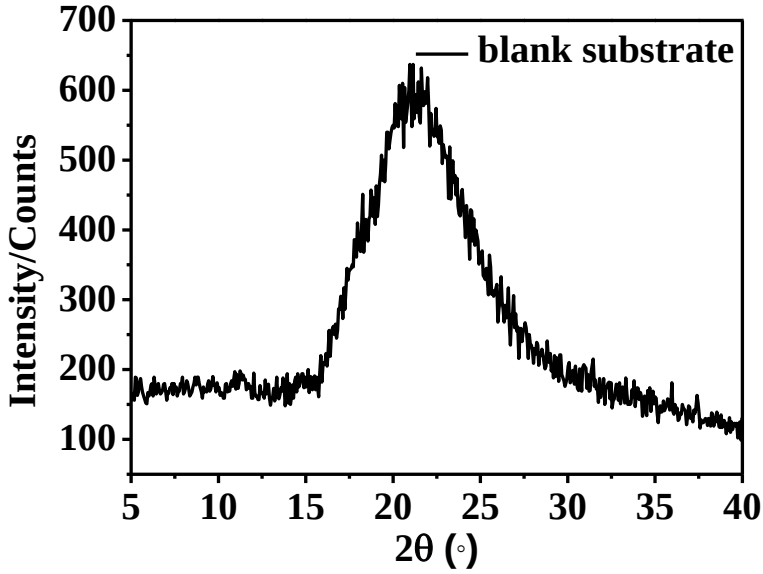

Figure S2. TGA thermograms of the four complexes.

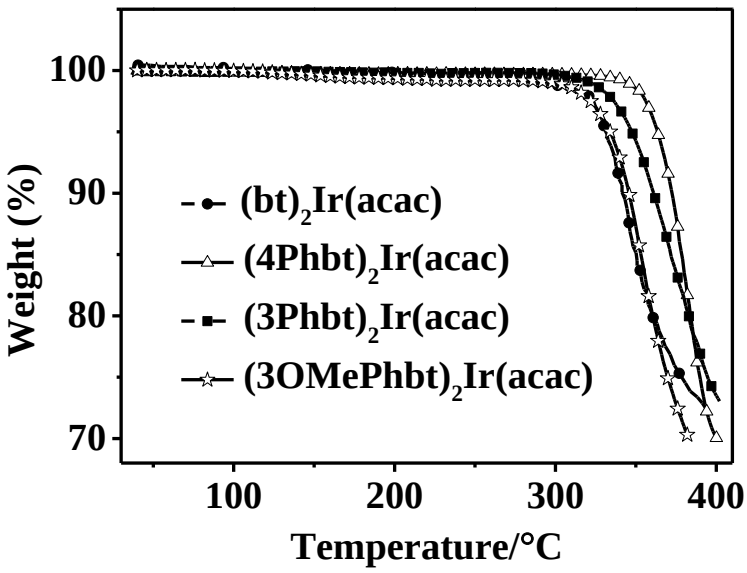

Figure S3. Polarized optical microscopy (POM) images of the polycrystalline samples of the four complexes under different temperatures. The photographs in the upper row are taken under polarized light, while those in the lower row are obtained under brightfield.

$(bt)_2Ir(acac)$

$(4Phbt)_2Ir(acac)$

$(3Phbt)_2Ir(acac)$

$(3OMePhbt)_2Ir(acac)$

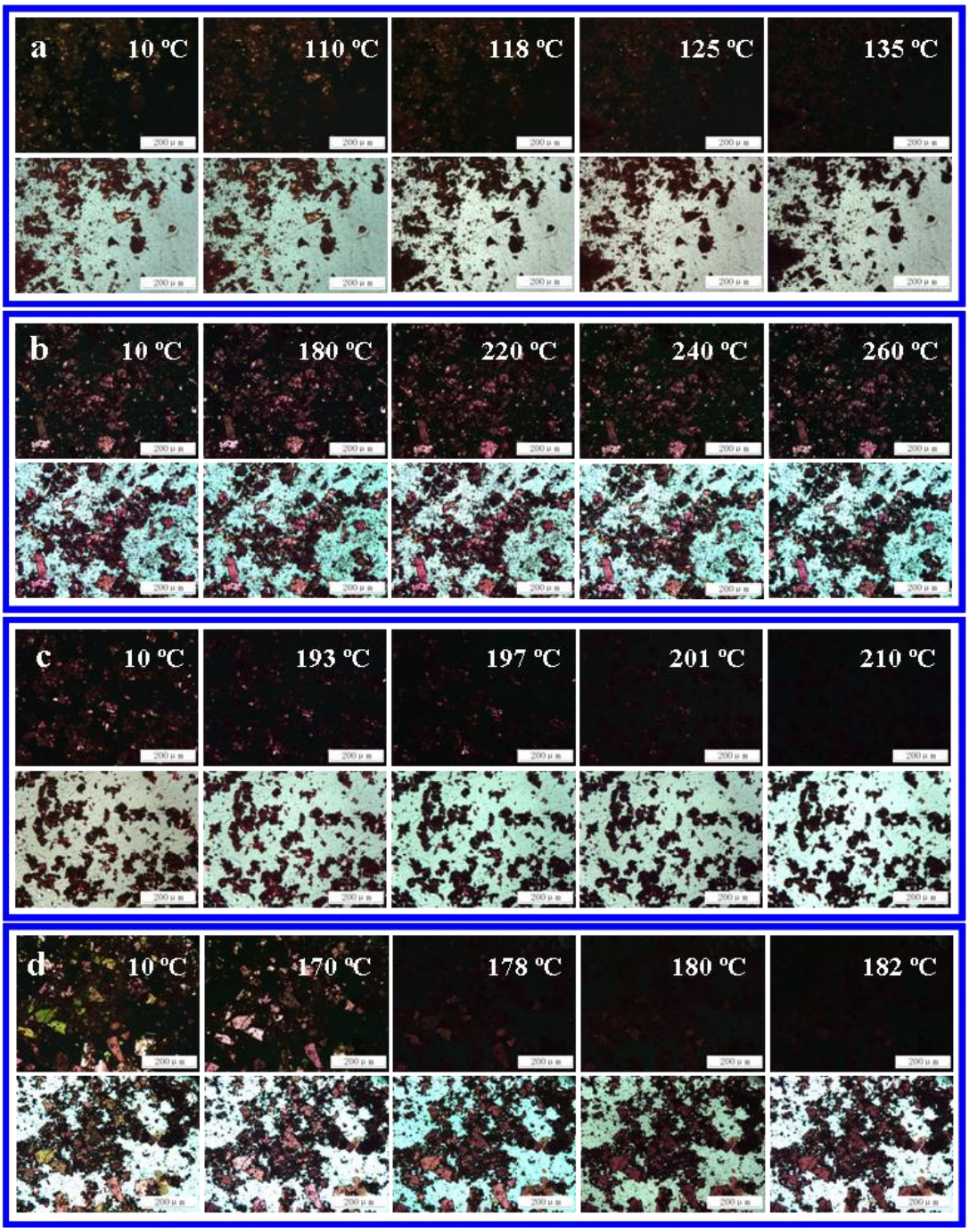

Figure S4. The **ORTEP** drawing and the crystal structures of **(bt)$_2$Ir(acac)**, **(4Phbt)$_2$Ir(acac)** and **(3Phbt)$_2$Ir(acac)**.

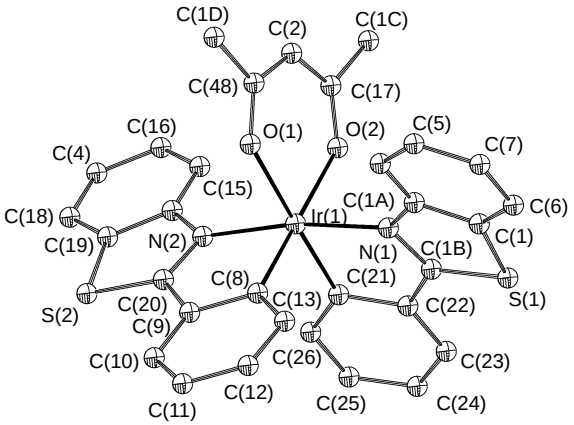

(bt)$_2$Ir(acac)

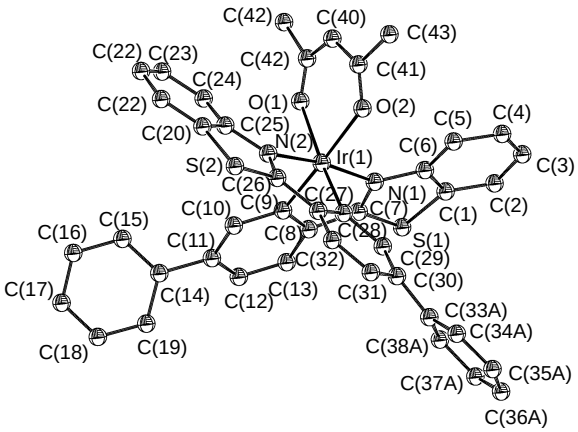

(4Phbt)$_2$Ir(acac)

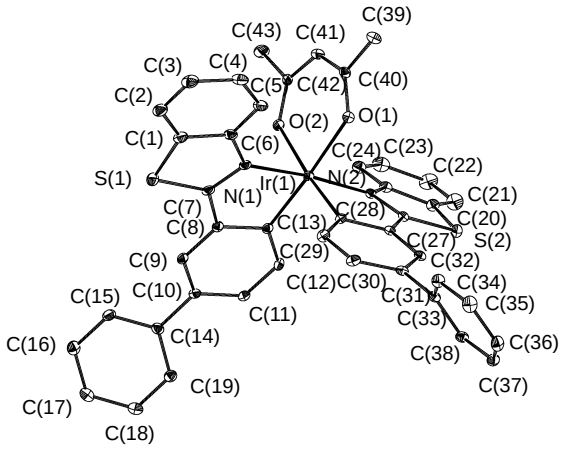

(3Phbt)$_2$Ir(acac)

Table S1. Crystal data and structure refinement for **$(bt)_2Ir(acac)$**, **$(4Phbt)_2Ir(acac)$**, and **$(3Phbt)_2Ir(acac)$**.

Compound	**$(bt)_2Ir(acac)\cdot C_6H_6$**	**$(4Phbt)_2Ir(acac)\cdot 2C_6H_6$**	**$(3Phbt)_2Ir(acac)$**
Empirical formula	$C_{37}H_{28}IrN_2O_2S_2$	$C_{55}H_{43}IrN_2O_2S_2$	$C_{43}H_{31}IrN_2O_2S_2$
Formula weight	788.93	1020.23	864.02
Temperature	130.0(10) K	150.1(2) K	130.0 K
Crystal system	Monoclinic	Triclinic	Monoclinic
Space group	$P2_1/c$	P-1	$P2_1/n$
a	14.8264(7) Å	12.4036(2) Å	17.3091(3) Å
b	15.4413(5) Å	12.4491(2) Å	12.6428(2) Å
c	13.7415(4) Å	16.4077(3) Å	18.5370(3) Å
α	90.00 deg	85.04(15) deg	90.00 deg
β	96.573(4) deg	70.7698(16) deg	95.9796(16) deg
γ	90.00 deg	68.67(16) deg	90.00 deg
Volume	3125.3(2) $Å^3$	2226.73(7) $Å^3$	4034.48(12) $Å^3$
Z	4	2	4
Calculated density	1.677 $mg\cdot mm^{-3}$	1.522 $mg\cdot mm^{-3}$	1.422 $mg\cdot mm^{-3}$
Absorption coefficient	4.443 mm^{-1}	3.137 mm^{-1}	3.448 mm^{-1}
F(000)	1556	1024	1712
Crystal size	0.40 × 0.35 × 0.35 mm	0.30 × 0.20 × 0.15 mm	0.32 × 0.29 × 0.25 mm
Reflections collected	8700	18767	17296
Independent reflections	4094 [R(int) = 0.0478]	9108 [R(int) = 0.0363]	8188 [R(int) = 0.0288]
θ-range for data collection	5.96 to 50°	2.89 to 26.37°	5.78 to 52.74°
Goodness-of-fit on F^2	0.964	1.052	1.052
Final R indices [I > 2σ (I)]	R_1 = 0.0350, wR_2 = 0.0797	R_1 = 0.0356, wR_2 = 0.0712	R_1 = 0.0312, wR_2 = 0.0639
R indices (all data)	R_1 = 0.0524, wR_2 = 0.0845	R_1 = 0.0440, wR_2 = 0.0745	R_1 = 0.0395, wR_2 = 0.0673
Largest diff. peak and hole	0.99 and -1.05 $e\cdot Å^{-3}$	1.15 and -0.89 $e\cdot Å^{-3}$	1.12 and -0.94 $e\cdot Å^{-3}$

Table S2. Selected bond lengths (Å) and angles (deg) for **$(bt)_2Ir(acac)$**, **$(4Phbt)_2Ir(acac)$** and **$(3Phbt)_2Ir(acac)$**.

Bond lengths (Å)		Bond angels (deg)	
		$(bt)_2Ir(acac)$	
Ir(1)-C(9)	1.991(8)	C(9)-Ir(1)-N(2)	92.50(2)
Ir(1)-C(22)	1.990(7)	C(22)-Ir(1)-N(1)	93.30(2)
Ir(1)-N(1)	2.059(5)	N(2)-Ir(1)-O(1)	170.90(2)
Ir(1)-N(2)	2.050(5)	N(2)-Ir(1)-N(1)	173.20(8)
Ir(1)-O(1)	2.158(4)	N(1)-Ir(1)-O(1)	86.85(19)
Ir(1)-O(2)	2.145(5)	O(2)-Ir(1)-O(1)	87.95(17)
O(1)-C(48)	1.248(8)	N(2)-Ir(1)-O(2)	86.57(19)
O(2)-C(17)	1.247(8)	N(1)-Ir(1)-O(2)	100.19(17)
		$(4Phbt)_2Ir(acac)$	
Ir(1)-C(9)	2.006(4)	C(9)-Ir(1)-N(2)	94.58(15)
Ir(1)-C(28)	2.002(4)	C(28)-Ir(1)-N(1)	93.83(16)
Ir(1)-N(1)	2.054(4)	N(2)-Ir(1)-O(1)	98.04(12)
Ir(1)-N(2)	2.042(4)	N(2)-Ir(1)-N(1)	172.47(13)
Ir(1)-O(1)	2.215(3)	N(1)-Ir(1)-O(1)	88.25(11)
Ir(1)-O(2)	2.165(3)	O(2)-Ir(1)-O(1)	86.21(12)
O(1)-C(39)	1.209(5)	N(2)-Ir(1)-O(2)	85.20(12)
O(2)-C(41)	1.204(5)	N(1)-Ir(1)-O(2)	99.40(13)
		$(3Phbt)_2Ir(acac)$	
Ir(1)-C(13)	1.998(4)	C(13)-Ir(1)- N(1)	80.80(13)
Ir(1)-C(28)	1.988(4)	C(28)-Ir(1)- N(2)	80.29(13)
Ir(1)-N(1)	2.057(3)	N(1)-Ir(1)-O(2)	85.37(11)
Ir(1)-N(2)	2.049(3)	N(1)-Ir(1)-O(1)	96.31(11)
Ir(1)-O(1)	2.136(2)	O(1)-Ir(1)-O(2)	88.96(10)
Ir(1)-O(2)	2.142(3)	N(2)-Ir(1)-N(1)	174.67(11)
O(1)-C(40)	1.280(4)	N(2)-Ir(1)-O(2)	98.15(10)
O(2)-C(42)	1.265(4)	N(2)-Ir(1)-O(1)	87.79(10)

Figure S5. Optimized structures and the numbering of important atoms of **(bt)$_2$Ir(acac)**, **(3Phbt)$_2$Ir(acac)** and **(3OMePhbt)$_2$Ir(acac)**. Calculations are conducted at the level of B3LYP/LANL2DZ/6-31(d,p).

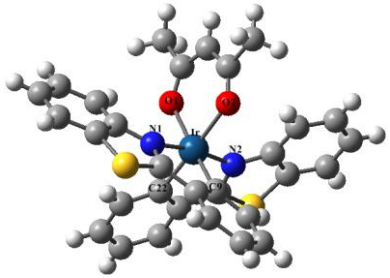

(bt)$_2$Ir(acac)

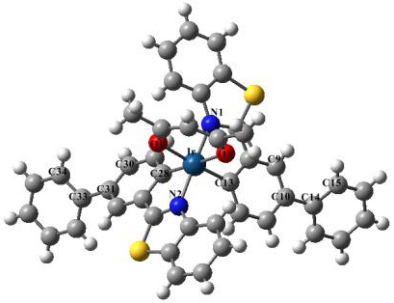

(3Phbt)$_2$Ir(acac)

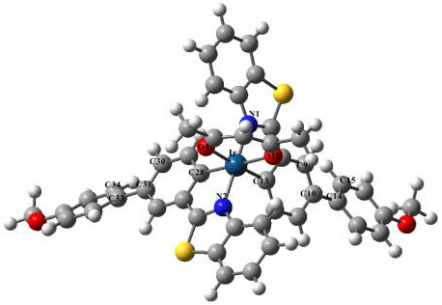

(3OMePhbt)$_2$Ir(acac)

Table S3. Optimized geometry parameters of the complexes using B3LYP method[a].

	$(bt)_2Ir(acac)$		**$(3Phbt)_2Ir(acac)$**	**$(3OMePhbt)_2Ir(acac)$**
		Bond Length (Å)		
Ir-O1	2.204 (2.158)	Ir(1)-O(1)	2.202 (2.200)	2.204
Ir-O2	2.204 (2.146)	Ir(1)-O(2)	2.202 (2.199)	2.202
Ir-N1	2.086 (2.059)	Ir(1)-N(1)	2.086 (2.085)	2.086
Ir-N2	2.086 (2.049)	Ir(1)-N(2)	2.089 (2.083)	2.088
Ir-C9	2.011 (1.990)	Ir(1)-C(13)	2.009 (2.007)	2.009
Ir-C22	2.011 (1.990)	Ir(1)-C(28)	2.208 (2.007)	2.008
		Bond Angle (deg)		
O1-Ir-O2	86.2 (87.9)	O1-Ir-O2	86.3 (86.3)	86.3
N2-Ir-N1	174.3 (170.9)	N1-Ir-N2	174.3 (174.7)	174.3
C9-Ir-C22	94.1 (91.2)	C13-Ir-C28	93.8 (94.4)	93.8
N2-Ir-C9	96.2 (92.5)	N2-Ir-C13	96.3 (96.3)	96.3
N1-Ir-C22	96.2 (93.3)	N1-Ir-C28	96.1 (96.5)	96.0
N2-Ir-C22	79.9 (80.5)	N2-Ir-C28	79.9 (79.9)	79.9
N1-Ir-C9	79.9 (80.9)	N1-Ir-C13	79.9 (79.9)	79.9
		Torsion Angle (deg)		
N1-Ir-C9-C22	-80.3 (-80.9)	N1-Ir-C13-C28	-95.7 (-95.9)	-95.5
N2-Ir-C22-C9	-80.3 (-80.6）	N2-Ir-C28-C13	-95.5 (-95.6)	-95.7
N1-Ir-C22-O1	-85.4 (-86.6）	N1-Ir-C28-O1	-99.0 (-98.7)	-98.7
N2-Ir-O1-C22	-96.2 (-92.7）	N2-Ir-O1-C28	-79.9 (-80.0)	-79.8
N1-Ir-O1-O2	-99.1 (-100.3）	N1-Ir-O1-O2	-84.8 (-84.7)	-84.6
N2-Ir-O2-O1	-99.1 (-99.8）	N2-Ir-O2-O1	-84.7 (-84.7)	-87.8
N1-Ir-O2-C9	-96.2 (-93.3）	N1-Ir-O2-C13	-79.9 (-79.9)	-79.9
N2-Ir-C9-O2	-85.4 (-86. 5)	N2-Ir-C13-O2	-98.7 (-98.5)	-99.1
C22-Ir-N1-O1	90.6 (91.5)	C28-Ir-N1-O1	90.7 (90.5)	91.2
C22-Ir-N2-O1	-90.8 (-91.4)	C28-Ir-N2-O1	-90.6 (-90.3)	-91.1
C9-Ir-N1-C22	93.1 (90.7)	C13-Ir-N1-C28	92.8 (93.4)	92.8
C9-Ir-N2-C22	-93.1 (-90.9)	C13-Ir-N2-C28	-92.8 (-93.4)	-92.7
O2-Ir-N1-C9	90.8 (90.4)	O2-Ir-N1-C13	90.9 (90.7)	90.5
O2-Ir-N2-C9	-90.7 (-90.4)	O2-Ir-N2-C13	-91.1 (-90.8)	-90.6
O1-Ir-N2-O2	85.4 (87.3)	O1-Ir-N1-O2	85.5 (85.5)	85.5
O1-Ir-N1-O2	-85.4 (-87.3)	O1-Ir-N2-O2	-85.5 (-85.5)	-85.5
C9-C10-C14-C15	/	C9-C10-C14-C15	36.5 (37.7)	-35.7
C30-C31-C33-C34	/	C30-C31-C33-C34	-36.6 (-37.7)	35.5

[a] The values in parentheses are derived from their corresponding crystal data.

Figure S6. UV-Vis absorption spectra of the complexes in CH_2Cl_2 solution and PL spectrum of PVK film (the illustration is an enlarged spectrum of the MLCT absorbance bands, PL spectrum is obtained under excitation of 340 nm).

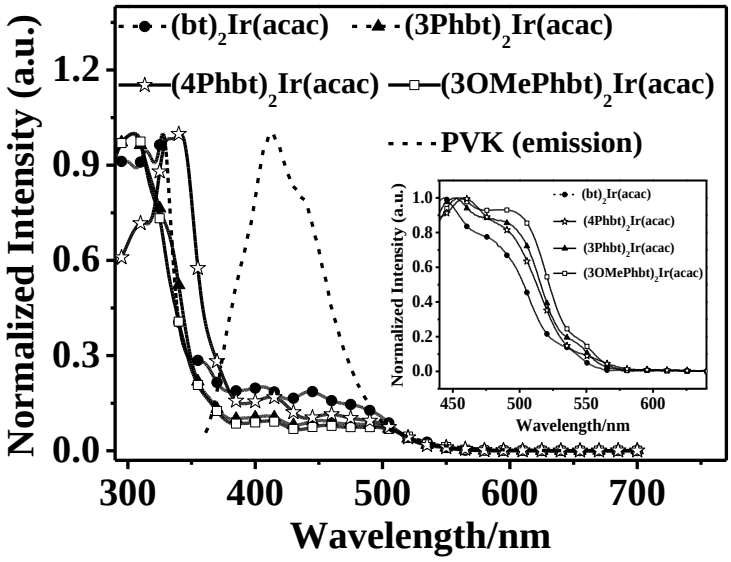

Figure S7. PL spectra of the blend films with (a) **$(bt)_2Ir(acac)$**, (b) **$(4Phbt)_2Ir(acac)$**, (c) **$(3Phbt)_2Ir(acac)$** and (d) **$(3OMePhbt)_2Ir(acac)$** doped in PVK at 1 wt%, 2 wt%, 6 wt% and 10 wt% (under excitation of 340 nm).

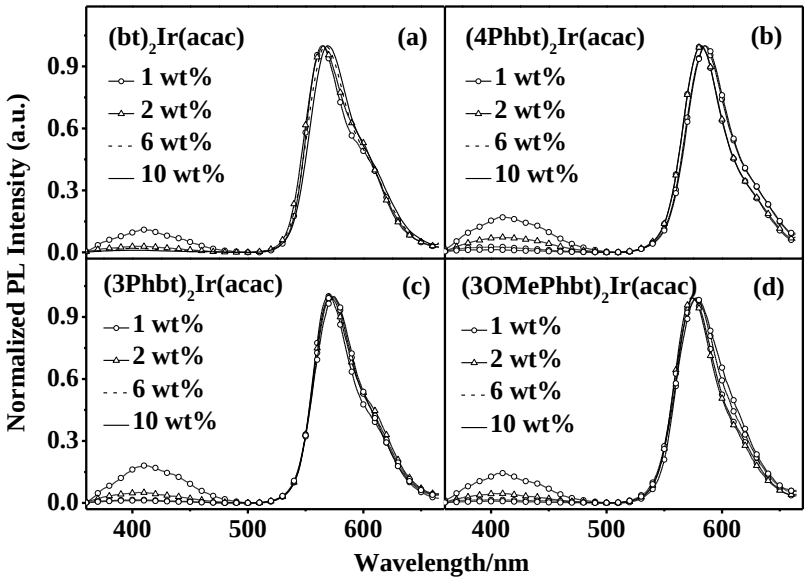

Figure S8. PL spectra of the blend films of PVK:OXD-7:Ir(III) complexes at 67 wt%: 27 wt%: 6 wt% level, neat OXD-7 and PVK film (under excitation of 340 nm).

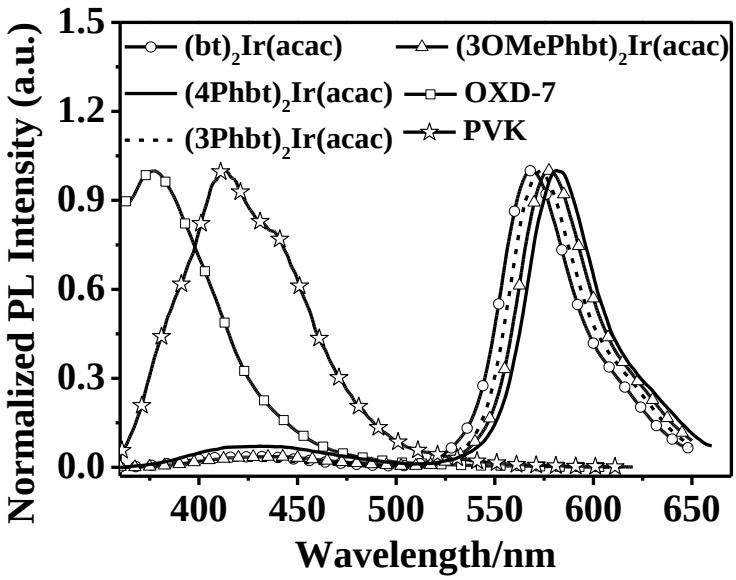

Figure S9. Cyclic voltammograms of **$(bt)_2Ir(acac)$**, **$(4Phbt)_2Ir(acac)$**, **$(3Phbt)_2Ir(acac)$** and **$(3OMePhbt)_2Ir(acac)$**. The oxidation potentials are determined relative to Ag/Ag^+ in 5×10^{-4} mol L^{-1} CH_2Cl_2 solution, using Fc/Fc^+ as internal reference.

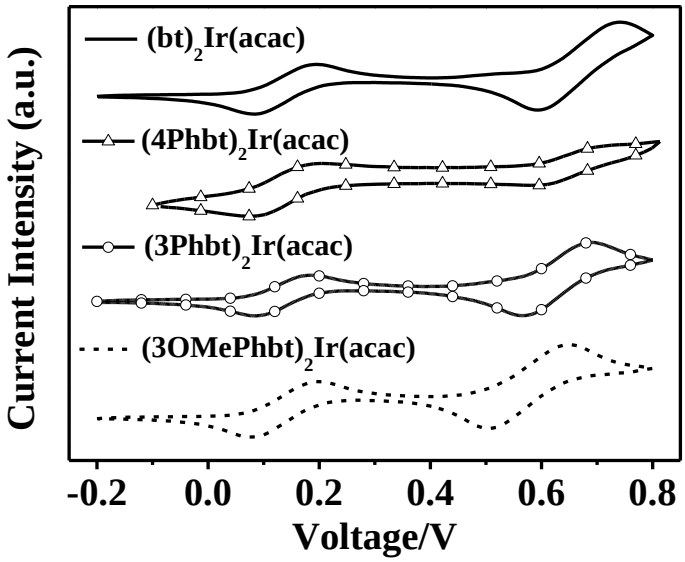

Figure S10. PL spectra of the blend films with (a) **(bt)$_2$Ir(acac)**, (b) **(4Phbt)$_2$Ir(acac)** (c) **(3Phbt)$_2$Ir(acac)** and (d) **(3OMePhbt)$_2$Ir(acac)** doped in PVK at 6 wt% level, and EL spectra of device I, II, III and IV.

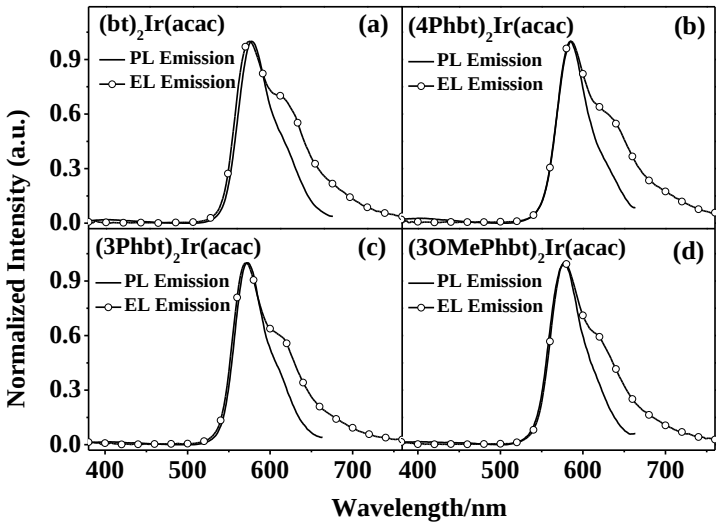

Figure S11. ^{1}H NMR of **(3Phbt)$_2$Ir(acac)** ($CDCl_3$, 400 MHz).

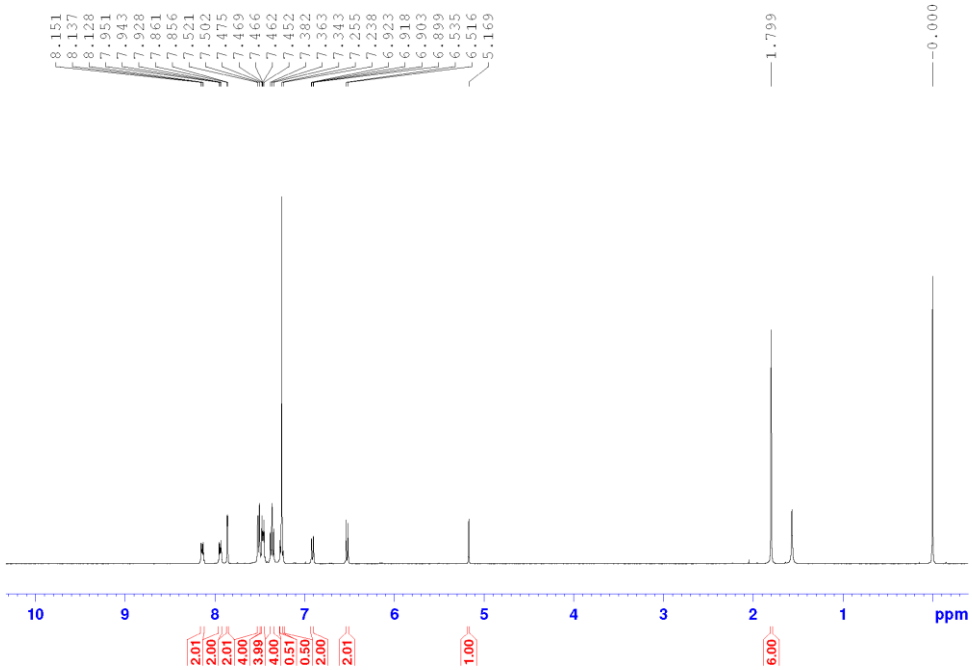

Figure S12. ^{1}H NMR of **(3OMePhbt)$_2$Ir(acac)** (DMSO-d_6, 400 MHz).

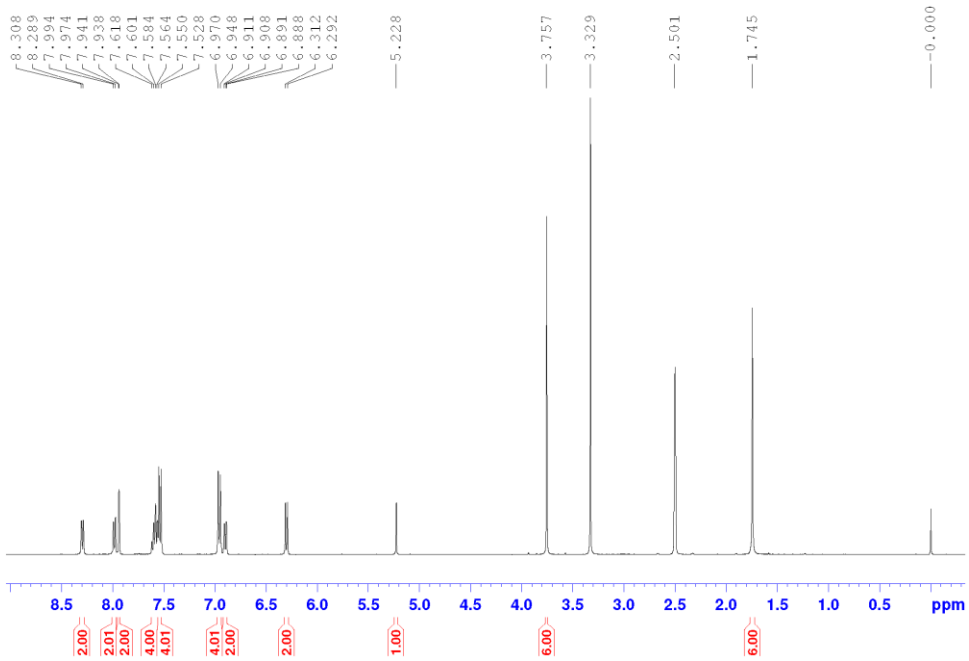

Figure S13. ^{13}C NMR of **(3Phbt)$_2$Ir(acac)** ($CDCl_3$, 100 MHz).

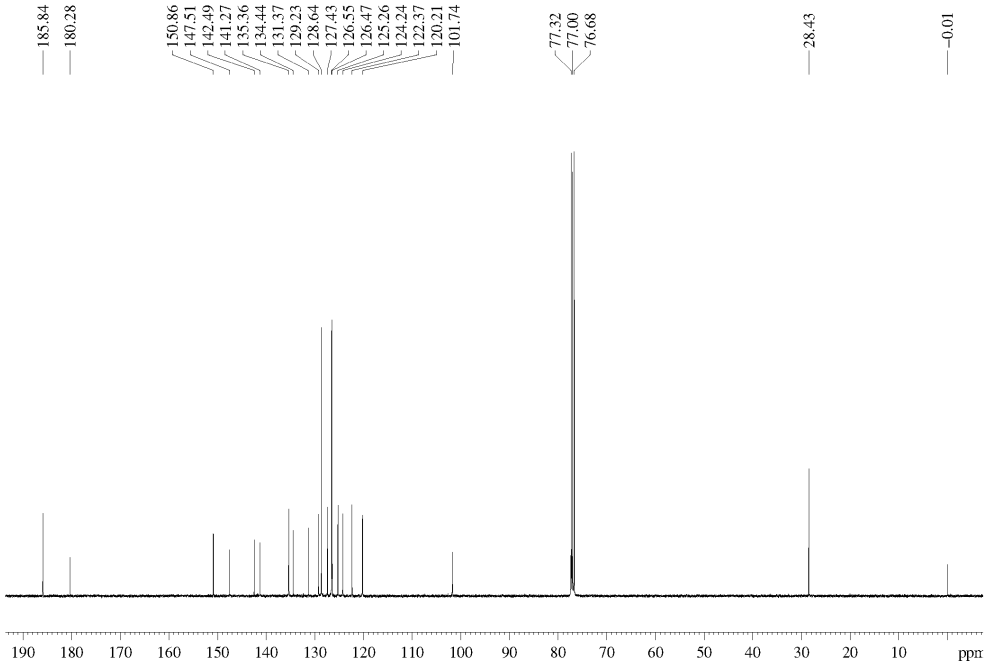

Figure S14. ^{13}C NMR of **(3OMePhbt)$_2$Ir(acac)** ($CDCl_3$, 100 MHz).

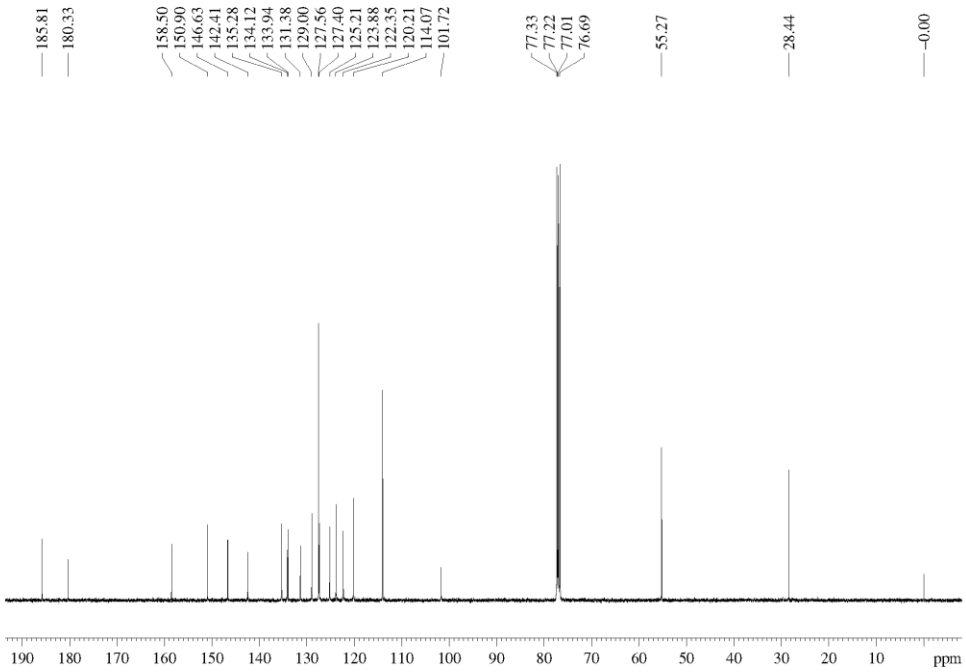

Figure S15. HR-ESI-MS spectrum of **(3Phbt)$_2$Ir(acac)** in CH_2Cl_2 solution.

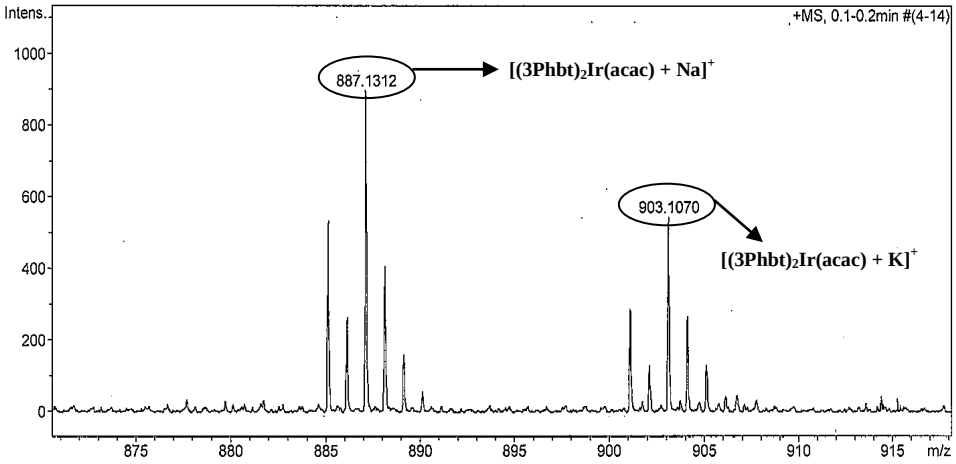

Figure S16. HR-ESI-MS spectrum of **(3OMePhbt)$_2$Ir(acac)** in CH_2Cl_2solution.